Growth of large-area graphene films from metal-carbon melts

Shaahin Amini,[1,a)] Javier Garay,[1] Guanxiong Liu,[2] Alexander A. Balandin,[2] and Reza Abbaschian[1]
[1]*Department of Mechanical Engineering, University of California–Riverside, Riverside, California 92507, USA*
[2]*Department of Electrical Engineering, University of California–Riverside, Riverside, California 92507, USA*

(Received 15 July 2010; accepted 1 September 2010; published online 10 November 2010)

We have demonstrated a new method for the large-area graphene growth, which can lead to a scalable low-cost high-throughput production technology. The method is based on growing single layer or few-layer graphene films from a molten phase. The process involves dissolving carbon inside a molten metal at a specified temperature and then allowing the dissolved carbon to nucleate and grow on top of the melt at a lower temperature. The examined metals for the metal-carbon melt included copper and nickel. For the latter, the high-quality single layer graphene was grown successfully. The resulting graphene layers were subjected to detailed microscopic and Raman spectroscopic characterization. The deconvolution of the Raman 2D band was used to accurately determine the number of atomic planes in the resulting graphene layers and access their quality. The results indicate that our technology can provide bulk graphite films, few-layer graphene as well as high-quality single layer graphene on metals. Our approach can also be used for producing graphene-metal thermal interface materials for thermal management applications. © *2010 American Institute of Physics*. [doi:10.1063/1.3498815]

I. INTRODUCTION

Graphene is a two-dimensional (2D) sheet of sp^2 bonded carbon atoms in a honeycomb network. The graphene crystal lattice is considered to be the basic building block of other important allotropes of carbonic materials: graphite, nanotubes, and fullerenes.[1] Recent investigations have established that graphene reveals a large number of unique properties including the quantum Hall effect at room temperature (RT),[2–5] ambipolar field effect,[6] high optical transparency,[7] extremely high electron mobility,[8–10] and capability for detection of single molecule via adsorption.[11] These physical properties stimulated active research of possible graphene device applications. From the practical point of view, some of the most interesting graphene properties are very high RT carrier mobility,[1,4,6,12] up to ~27 000 $cm^2\ V^{-1}\ s^{-1}$ and most recently discovered high thermal conductivity[13–16] exceeding ~3000 W/m K at RT for the large suspended graphene flakes. The enhanced current and heat conduction properties are beneficial for electronic, interconnect, and thermal management applications of graphene. It has also been demonstrated that graphene devices can operate at very low-levels of the electronic flicker noise, which is important for applications in sensors and communications.[17–19]

However, any commercial applications of graphene would require a reliable, scalable, and low-cost synthesis technique. In order to be suitable for industrial applications the technique should satisfy a number of requirements. First, with the technique, one should be able to produce high-quality 2D crystals to ensure high carrier mobility and thermal conductivity. Second, the technique should provide means for growing few-layer graphene (FLG) and opportunity for the fine control of the film thickness. Third, the technique should be scalable. Among several existing techniques,[20,21] the most successful method that has resulted in isolation of the high-quality single layer graphene (SLG) is the mechanical exfoliation (micromechanical cleavage).[6] Other demonstrated techniques include the epitaxial growth,[22–24] chemical vapor deposition (CVD),[25–27] chemically derived graphene from graphite oxide,[28,29] and high pressure-high temperature growth.[30] The mechanical exfoliation, while suitable for laboratory research, is unlikely to become practical for commercial applications. The graphene growth by CVD is promising but still has a number of problems related to control of the thickness and quality. The existing techniques have other drawbacks resulting from large equipment cost and long processing times.

Here, we propose a completely different approach for graphene growth. Our technique is low cost and scalable which utilizes standard equipment available in industry. The technique is capable of producing high-quality FLG and SLG. The process involves dissolution of carbon atoms in a molten metal, followed by cooling the melt to allow the dissolved atoms precipitation on top on the melt as SLG. In this paper we describe the technique and physical properties of the obtained materials.

II. EXPERIMENTAL PROCEDURES

Our technique is based on dissolving carbon atoms in a transition metal melt at a certain temperature and then allowing the dissolved carbon to precipitate out at a lower temperature as SLG. The schematic of the process with nickel is shown in Fig. 1. In Fig. 1(a) nickel is melted in contact with a carbon source. This source could be the graphite crucible

a)Electronic mail: samini@engr.ucr.edu.

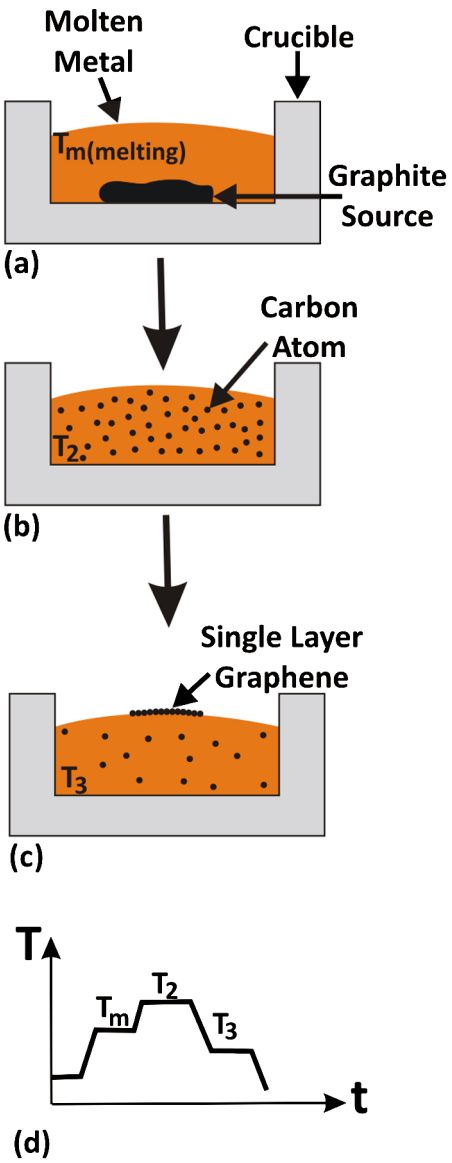

FIG. 1. (Color online) Schematic of graphene growth from molten nickel (a) melting nickel in contact with graphite as carbon source, (b) dissolution of carbon inside the melt at high temperatures, and (c) reducing the temperature for growth of graphene. (d) shows temperature-time diagram of the process.

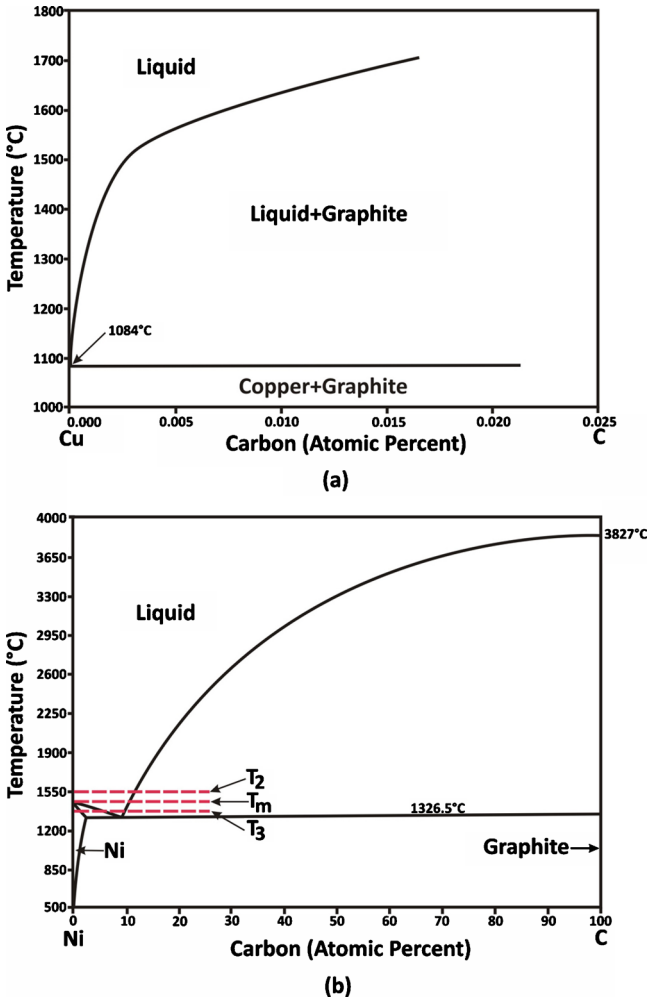

FIG. 2. (Color online) Phase diagrams of selected binary systems: Cu–C (a) and Ni–C (b), the processing temperatures of Fig. 1 are marked in the Ni–C phase diagram.

inside which the melting process is carried out or intentionally added graphite chunk or powder to the melt. Keeping the melt in contact with carbon source at a given temperature results in dissolution and saturation of carbon atoms in the melt. The process is described by the binary phase diagram of metal-carbon [Fig. 1(b)]. Upon lowering the temperature, the solubility of carbon in the molten metal decreases and the excess amount of carbon precipitates on top of the melt [Fig. 1(c)]. The temperature-time diagram of the process is shown in Fig. 1(d). The floating layer can be either skimmed or allowed to freeze for subsequent removal.

The described processing technique was utilized with copper and nickel (see the corresponding phase diagrams in Fig. 2). For convenience, the processing temperatures, indicated in Fig. 1, are also shown in Fig. 2(b). The arc melting process and melting in resistance furnace were selected for the dissolving process. For the former technique the direct-current electrode negative process was used. The processing chamber was vacuumed and then backfilled with argon for two times. The current was chosen to be 75 A and the melting process was carried out for 20 s. In the resistance furnace technique, the furnace was first vacuumed to 10^{-6} torr and then backfilled with the purified argon. After reaching 1500 °C, the samples were kept for 16 h and then cooled to the ambient temperature. Both heating and cooling rates were 10 °C/min. For Cu–C system, the melting process was carried out in the graphite crucibles as the carbon source. In Ni–C system a hypereutectic composition of Ni +2.35 wt % C was selected and the specified amount of carbon was added to the molten metal in the form of chunk graphite.

The obtained samples were investigated with optical microscopy, scanning electron microscopy (SEM) and micro-Raman spectroscopy. Additional studies were carried out by dissolving the metal substrate away and transferring the graphene layers to a silicon wafer using the method previously reported for the transfer of carbon nanotubes and graphene layers.[25,31] To achieve this, a layer of poly methyl methacrylate (PMMA) was spin coated on the substrate

(1800 rpm for 30 s). The metal substrate was etched away by a nitric acid solution (1:2) allowing the PMMA/carbonic layer to float on top of the solution. At the next step, the layer was placed on a glass substrate and washed with isopropanol and water. The dual layer of PMMA and carbonic layer were then transferred to a Si/SiO_2 wafer. The film was annealed at 60 °C for 1 h to adhere firmly to the target substrate. The PMMA was dissolved with the acetone drops gradually and the carbonic layers were left on the substrate. The wafer with the carbonic layers was washed with isopropanol and dried with the nitrogen gas.

The Raman spectra were taken using a Horiba Jobon Yvon micro-Raman spectrometer. All spectra were excited with the visible (632.8 nm) laser light (power 3.6 mW) and collected in the backscattering configuration. The spectra were recorded with the 1800 lines/mm grating. A 100× objective was used to focus the excitation laser light on different spots of the samples. Raman spectroscopy has been utilized as a convenient technique for identifying and counting graphene atomic layers.[32–35] The most prominent features in the Raman spectra of graphitic materials are the G band (~1582 cm^{-1}), D band (~1350 cm^{-1}), D′ band (~1620 cm^{-1}), and the 2D band (~2700 cm^{-1}).[32,36] The G band is Raman active for sp^2 carbon networks. In contrast, sp^3 and sp carbon show characteristic Raman features at 1333 cm^{-1} (diamond) and in the range 1850–2100 cm^{-1} (linear carbon chains), respectively. The D and D′ bands are the defect induced Raman features. For this reason, the D bands cannot be seen for highly crystalline graphite without defect. The integrated intensity ratio for the D band and G band (I_D/I_G) is widely used for characterizing the defect quantity in graphitic materials. The 2D (or G′) band corresponds to the overtone of the D band observed in all kinds of graphitic materials and exhibit a strong Raman band which appears in the range 2500–2800 cm^{-1}. It has been shown[32] that the evolution of the 2D band Raman signatures with the addition of each extra layer of graphene can be used to accurately count the number of layers. A rough estimate on the number of layers can also be obtained from analysis of I_G/I_{2D} ratio.[32,37] What is also important for our analysis is that graphene identification by means of micro-Raman spectroscopy is reliable on various substrates (not only on Si/SiO_2).[38,39] It has also been shown that among the metallic substrates, nickel is an appropriate one for direct Raman Spectroscopy investigation.[26]

III. RESULTS AND DISCUSSION

The goal of this process is to grow controllably SLG and FLG. A calculation based on the lever rule[40] on Cu–C phase diagram shows that cooling from 1200 and 1800 °C to the melting point of copper (1080 °C) results in the formation of layers with the thickness ranging from several nanometers to several micrometers, respectively. Selecting the higher alloying temperatures leads to dissolution of more carbon atoms in the melt and, consequently, larger amount of carbon precipitating on the melt upon cooling. The latter will result in the formation of a thicker graphite layer. Nevertheless, the precipitated graphite layer on the melt may not be uniform and its thickness varies from SLG to bulk graphite. The described type of the thickness control is more suitable for FLG or thicker graphite layers.

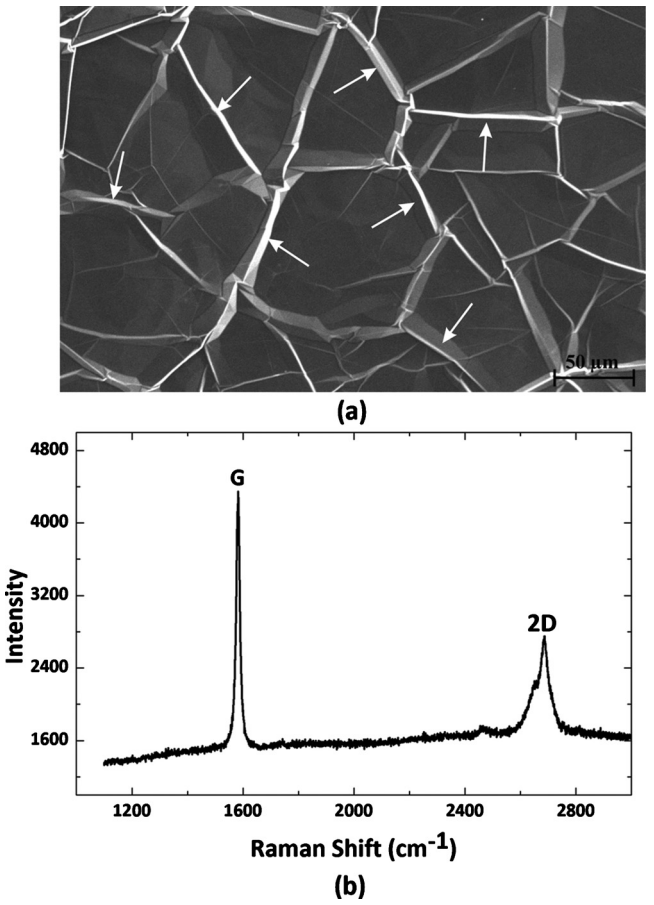

FIG. 3. SEM photo (secondary electron image) of thick graphite layer formed on top of the nickel (a) and its Raman spectrum (b), the arrows show the wrinkles.

Figure 3(a) shows the graphite layer, which has been formed on top of nickel. The film has a specific morphology of smooth surface areas separated from each other by the out-of-plane faceted ridges. The areas, which separate the flat regions, are referred to as wrinkles or creases, and are marked with the white arrows in Fig. 3(a). The typical size of the smooth surface regions was found to be around 50 μm. Figure 3(b) demonstrates a typical Raman spectrum of the smooth areas. The spectrum reveals an intense G peak at 1583 cm^{-1} and an asymmetric 2D band with a shoulder centered at 2651 cm^{-1} and the main peak centered at 2686 cm^{-1}. No disorder induced D or D′ bands were observed in the spectra. Similiary, Raman spectra were recorded from other smooth areas and the results were identical. The Raman spectrum features shown in Fig. 3(b) are similar to those of bulk crystalline graphite reported in literature.[32] This is in line with the phase diagram data. Indeed, from the phase diagram, one can see that for the selected Ni–C composition (hypereutectic alloy of Ni +2.35 wt % C), upon cooling of the molten phase, a graphite shell should grow on top of the melt as the primary graphite. The surface of the melt is a favorable site for heterogeneous nucleation and growth of graphite films.

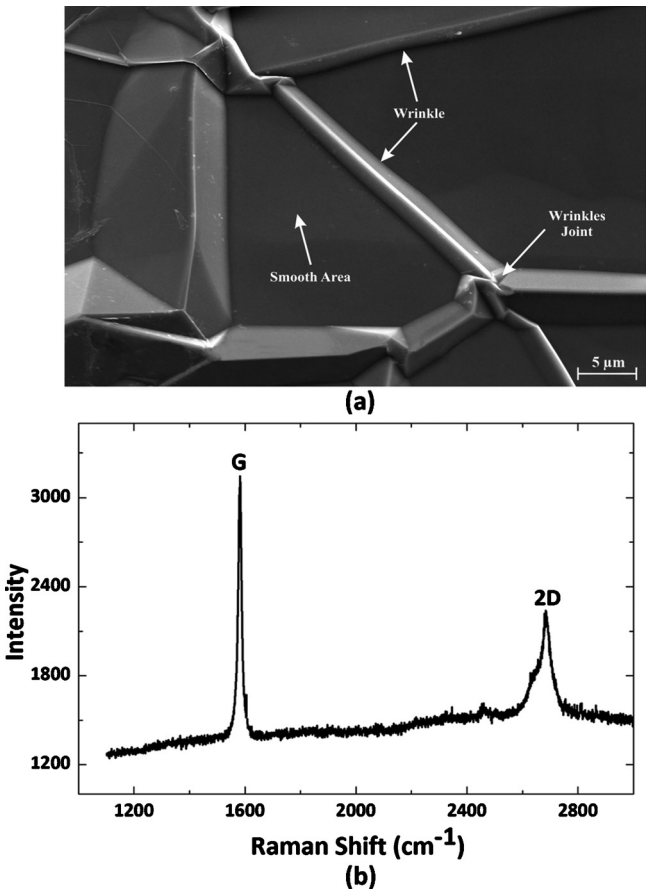

FIG. 4. SEM photo (secondary electron image) of a graphite smooth area bounded by wrinkles on top of nickel substrate (a) and the Raman spectrum of a wrinkle(b).

In Fig. 4(a), we present the magnified view of a flat area of another Ni+2.35 wt % C sample, which is bounded by four wrinkles with triangular cross-sections. The joint between the creases has a more complicated microstructure but the faceted structure is still evident. In Fig. 4(b), we present the Raman spectrum recorded from a crease. The micro-Raman spectroscopy reveals the intense G peak at 1582 cm^{-1} and an asymmetric 2D band with a shoulder at 2650 cm^{-1} and a main peak at 2684 cm^{-1}. No D and D′ bands could be observed in the spectrum. The wrinkled feature of the graphite layers is believed to be due to accommodation of the differences in the thermal expansion coefficients between the metal substrate and the graphite layer.[41] After the formation of the graphite shell on top of the melt and conclusion of the eutectic reaction both nickel and graphite contract as the sample cools down. The thermal expansion coefficient of nickel[42] varies from 21.0 to 12.89 $\times 10^{-6}$ K^{-1} for the temperature range from 1200 to 27 °C while the in-plane thermal expansion coefficient of graphite[43] changes from 1.25 to -1.25×10^{-6} K^{-1} for the same temperature range. This difference in the thermal expansion coefficients gives rise to a larger lateral contraction of the metal substrate than that of graphite film. As a result, a compressive biaxial stress[41] will develop on the graphite layer which consequently leads to the formation of triangular folds in the film. The wrinkle formation is schematically shown in Fig. 5. The *ab initio* studies[43] as well as experimental results[44,45] indicate that the bulk graphite below 400 °C and SLG possess negative thermal coefficient that intensify the thermal coefficient expansion mismatch even further.

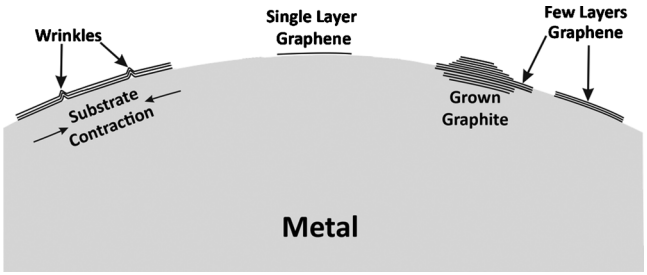

FIG. 5. Schematic of wrinkle, SLG and a FLG formation.

From comparison of the Raman spectral features in the smooth areas and wrinkles [see Figs. 3(b) and 4(b)] one can conclude that the structure of the wrinkles is identical to flat areas. In fact, the wrinkles are part of the graphite films, which form during the cooling process, and have the same crystal structure as the flat areas. The facets in the wrinkle joint in Fig. 4(a) demonstrate the crystalline structure of the wrinkles. It is believed that the weak van der Waals forces among the graphene layers allow them to simply shift upward under the biaxial stresses. Although the individual layers are rather stable owing to the strong covalent bonds, the graphene layers can bend or fold without losing their crystal structure. The absence of the disorder D and D′ bands in these spectra also shows that the deformed layer with its creases is free of defects. It has been shown that deformation of graphene layers and formation of the creases are due to kinking[46] or twining.[47] The strong in-plane covalent bonds and the resilient structure of graphite are comprehended by the formation of these wrinkles.

A few layers graphene can also precipitate from the melt. Figure 6 shows SEM image of the electron transparent graphitic layer on copper. The layer is thin enough to serve as a window for 5 keV electrons to pass along. FLG can also be formed at the edges of thick graphite. By transferring the graphitic layers to Si/SiO_2 substrates we found that the color contrast at the edges of precipitated graphite islands is different. Thus, there is a possibility of finding FLG at the edges. As a graphitic layer nucleates on the melt it expands

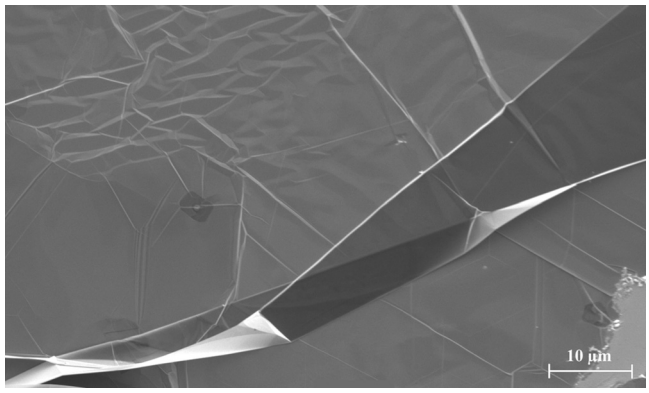

FIG. 6. SEM photo (secondary electron image) of a transparent graphitic layer on copper.

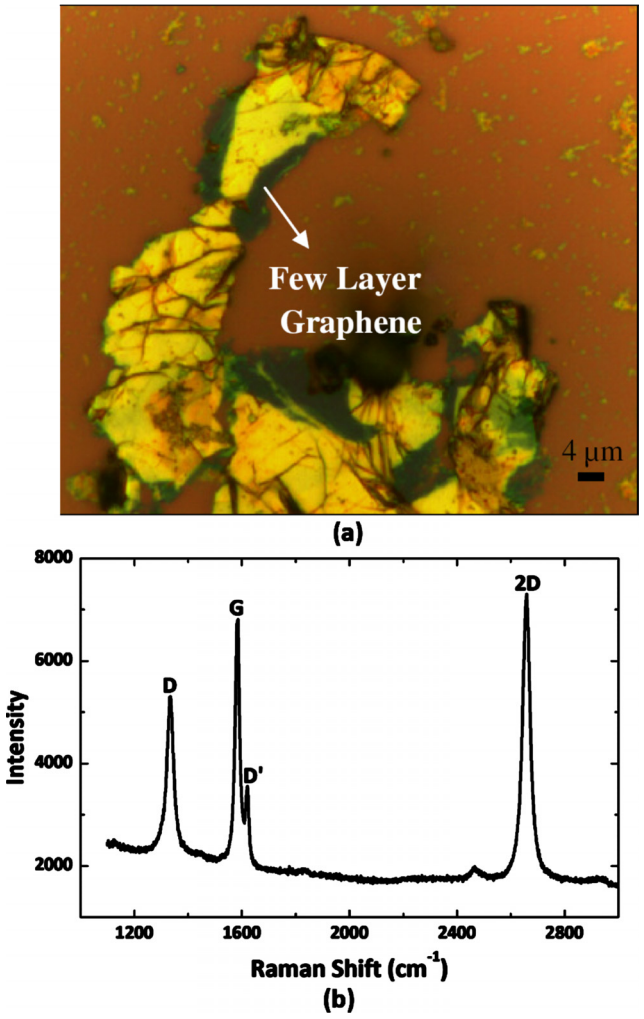

FIG. 7. (Color online) Optical microcopy of few layer graphene formed on top of copper and then transferred to Si/SiO_2 (a) and its Raman spectrum (b).

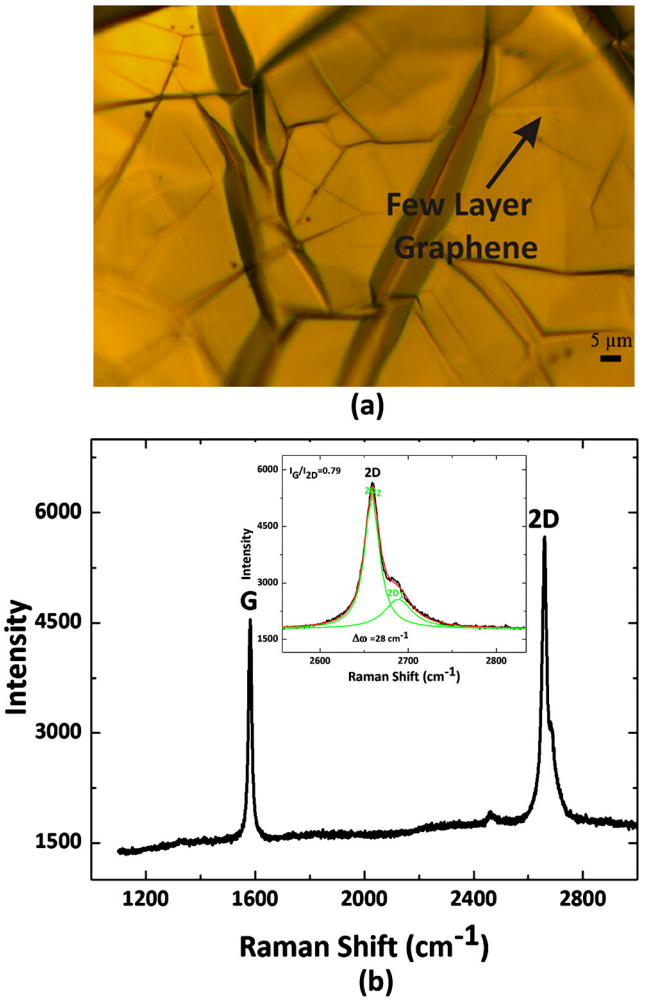

FIG. 8. (Color online) Optical microcopy of few layer graphene formed on top of nickel (a) and Raman spectrum of the formed layer and its 2D band deconvolution (b).

laterally and normally and the island edges could be as thin as FLG. The schematic of this mechanism is shown in Fig. 5. One of the islands grown on copper and the Raman spectrum of its edge are presented in Fig. 7. The spectrum features a symmetric 2D band and intense D and D′ bands. The I_G/I_{2D} ratio indicate the presence of 5–6 layers graphene.[33] The symmetric 2D band suggest a possibility of forming turbostratic graphite (i.e., without ABAB stacking).[32]

The intense D and D′ peaks indicate the layers with a large number of defects.[36] It is reasonable to explain the defect formation by the entrapment of the high-temperature vacancies owing to the high cooling rate of copper. The thermal expansion coefficient mismatch between the substrate and graphite also gives rise to the formation of cracks. These defect formation mechanisms cause intense D and D′ peaks observed in Raman spectrum in Fig. 7. An area of the FLG on nickel and its Raman spectrum are shown in Fig. 8. The 2D band has been deconvoluted (Lorentzian analysis) for examining the number of layers. The Raman spectrum shows a G band at 1583 cm^{-1}. The 2D band deconvolution reveals two Lorentzian peaks at $2D_1=2688$ cm^{-1} and $2D_2=2660$ cm^{-1} ($\Delta\omega=28$ cm^{-1}). The Raman spectrum analysis suggests the presence of four-layer graphene.[38,48] The missing D and D′ bands indicate the defect-free FLG on nickel. This is dissimilar to the FLG forming on copper. The thermal diffusivity of copper is nearly five times of nickel.[49] The higher thermal diffusivity of copper leads to higher cooling rate and consequently more intense defect formation.

It is interesting to note that, as the substrate, nickel has not strongly affected the Raman features of graphene. The Raman spectrum of SLG was detected in many spots on top of nickel. A pristine SLG and its Raman spectrum are shown in Fig. 9. The area of the grown SLG is larger than 125 μm^2. The Raman spectrum shows G band at 1583 cm^{-1} and an symmetric 2D band at 2660 cm^{-1}. The absence of D peak proves that the formed SLG is high-quality and defect-free. The full length at half maximum for 2D peak of the grown SLG is 17 cm^{-1} (as compared to the reported value of 25 cm^{-1}).[32] The I_G/I_{2D} ratio is 4.53 and the deconvolution of 2D band indicates a complete symmetry as it is expected for SLG.

The amount of graphite forming on the melt and its characteristic depend strongly on the quantity of carbon dissolved in the melt and the solubility limit of carbon in the liquid as well as the selected cooling conditions. For the present investigation the two alloy systems of Cu–C and

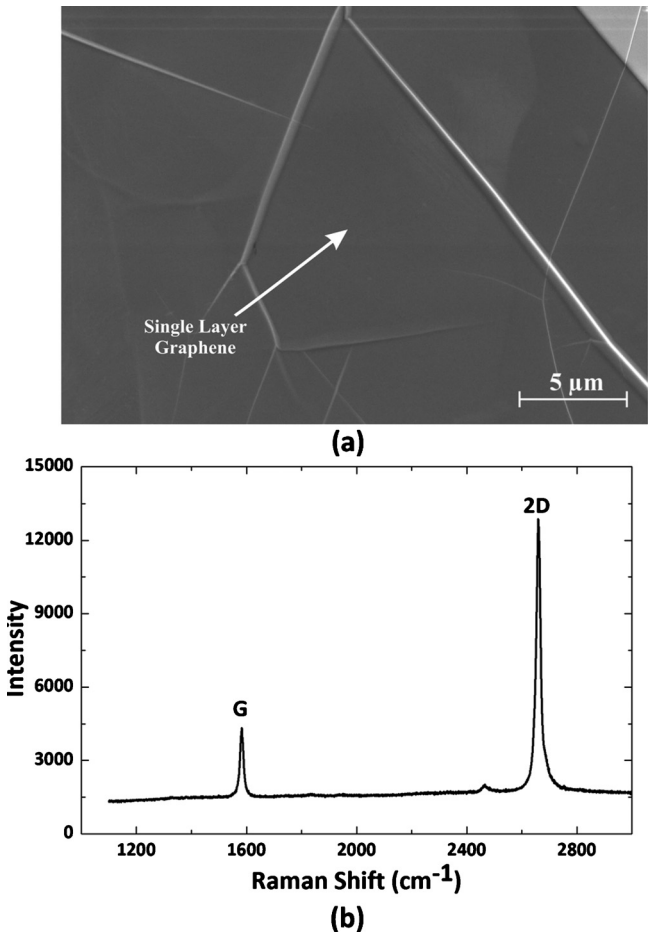

FIG. 9. SEM photo of SLG formed on nickel (a) and its Raman spectrum (b).

Ni–C show substantial differences in the solubility limits.[50,51] It approves that the Ni–C system is more suitable for the formation of large and defect-free layers. However, additional studies are needed to specify the differences.

One should mention here that the formation, structure and energetics of the growth of SLG and FLG from molten metal have many features in common with the monolayer and multilayer carbon formation by segregation and precipitation from the bulk solid solutions. In particular, the data on the equilibrium segregation of carbon to nickel surface and carbon interaction with nickel surfaces investigated in details and reported by Blakely and co-workers[52–58] can be used for optimization of graphene growth from the metal-carbon melts proposed in this work. The orientation and texture of the surface layers are currently under investigation, and the results will be described in a follow-up publication.

The developed technology can lead to applications of the resulting graphene-metal composites as thermal interface materials (TIMs) for heat dissipation in electronic chips and other devices. The layered graphene-metal composites are expected to have enhanced thermal conductivity exceeding that of metals.[13,14] The improved thermal management and advanced TIMs are currently important areas of research due to increasing power dissipation in state-of-the-art electronic, optoelectronic, and photonic devices.[59]

IV. CONCLUSIONS

We proposed a new approach for growing large-area FLG and SLG films. The technique involved dissolution of carbon in a molten metal at a specified temperature and then allowing the dissolved carbon atoms to nucleate and grow on top of the melt at a lower temperature. The detailed microscopy and micro-Raman spectroscopy were utilized to characterize the obtained layers. Different morphologies including thick graphite, FLG and SLG were observed on metal substrates. The bulk graphite microstructure shows the flat areas bounded by the triangular faceted wrinkles formed due to the mismatch in the thermal expansion coefficients of the metal substrate and graphite. FLG was also grown on both nickel and copper substrate. The Raman spectroscopy proved that SLG larger than 125 μm^2 has been successfully grown on nickel substrate. The absence of the D and D′ bands in the Raman spectrum of SLG indicates graphene's high-quality. We found that nickel provides a better substrate for growing SLG from the melt. The graphene-metal composites produced by this technique can be utilized as TIMs in a variety of applications.

ACKNOWLEDGMENTS

The authors wish to thank Dr. Shahram Amini of the National Hypersonic Science Center with University of California Santa Barbara for his support and comments. A.A.B. acknowledges support from DARPA—SRC Focus Center Research Program (FCRP) through its Center on Functional Engineered Nano Architectonics (FENA) and Interconnect Focus Center (IFC).

[1] A. K. Geim and K. S. Novoselov, Nature Mater. **6**, 183 (2007).
[2] K. S. Novoselov, E. McCann, S. V. Morozov, V. I. Falko, M. I. Katsnelson, U. Zeitler, D. Jiang, F. Schedin, and A. K. Geim, Nat. Phys. **2**, 177 (2006).
[3] Z. Jiang, Y. Zhang, Y. W. Tan, H. L. Stormer, and P. Kim, Solid State Commun. **143**, 14 (2007).
[4] Y. Zhang, Y.-W. Tan, H. L. Stormer, and P. Kim, Nature (London) **438**, 201 (2005).
[5] D. A. Abanin, K. S. Novoselov, U. Zeitler, P. A. Lee, A. K. Geim, and L. S. Levitov, Phys. Rev. Lett. **98**, 196806 (2007).
[6] K. S. Novoselov, A. K. Geim, S. V. Morozov, D. Jiang, Y. Zhang, S. V. Dubonos, I. V. Grigorieva, and A. A. Firsov, Science **306**, 666 (2004).
[7] R. R. Nair, P. Blake, A. N. Grigorenko, K. S. Novoselov, T. J. Booth, T. Stauber, N. M. R. Peres, and A. K. Geim, Science **320**, 1308 (2008).
[8] M. Han, B. Ozyilmaz, Y. Zhang, P. Jarillo-Herero, and P. Kim, Phys. Status Solidi B **244**, 4134 (2007).
[9] K. I. Bolotin, K. J. Sikes, Z. Jiang, M. Klima, G. Fudenberg, J. Hone, P. Kim, and H. L. Stormer, Solid State Commun. **146**, 351 (2008).
[10] S. V. Morozov, K. S. Novoselov, M. I. Katsnelson, F. Schedin, D. C. Elias, J. A. Jaszczak, and A. K. Geim, Phys. Rev. Lett. **100**, 016602 (2008).
[11] F. Schedin, A. K. Geim, S. V. Morozov, E. W. Hill, P. Blake, M. I. Katsnelson, and K. S. Novoselov, Nature Mater. **6**, 652 (2007).
[12] C. Berger, Z. Song, X. Li, X. Wu, N. Brown, C. Naud, D. Mayou, T. Li, J. Hass, A. N. Marchenkov, E. H. Conrad, P. N. First, and W. A. de Heer, Science **312**, 1191 (2006).
[13] A. A. Balandin, S. Ghosh, W. Bao, I. Calizo, D. Teweldebrhan, F. Miao, and C. N. Lau, Nano Lett. **8**, 902 (2008).
[14] S. Ghosh, I. Calizo, D. Teweldebrhan, E. P. Pokatilov, D. L. Nika, A. A. Balandin, W. Bao, F. Miao, and C. N. Lau, Appl. Phys. Lett. **92**, 151911 (2008).
[15] S. Ghosh, W. Bao, D. L. Nika, S. Subrina, E. P. Pokatilov, C. N. Lau, and A. A. Balandin, Nature Mater. **9**, 555 (2010).
[16] D. L. Nika, E. P. Pokatilov, A. S. Askerov, and A. A. Balandin, Phys. Rev. B **79**, 155413 (2009).

[17]Y.-M. Lin and P. Avouris, Nano Lett. **8**, 2119 (2008).
[18]Q. Shao, G. Liu, D. Teweldebrhan, A. A. Balandin, S. Rumyantsev, M. S. Shur, and Y. Dong, IEEE Electron Device Lett. **30**, 288 (2009).
[19]G. Liu, W. Stillman, S. Rumyantsev, Q. Shao, M. Shur, and A. A. Balandin, Appl. Phys. Lett. **95**, 033103 (2009).
[20]X. Lu, M. Yu, H. Huang, and R. S. Ruoff, Nanotechnology **10**, 269 (1999).
[21]A. M. Affoune, B. L. V. Prasad, H. Sato, T. Enoki, Y. Kaburagi, and Y. Hishiyama, Chem. Phys. Lett. **348**, 17 (2001).
[22]C. Berger, Z. Song, T. Li, X. Li, A. Y. Ogbazghi, R. Feng, Z. Dai, A. N. Marchenkov, E. H. Conrad, P. N. First, and W. A. de Heer, J. Phys. Chem. B **108**, 19912 (2004).
[23]C. Berger, Z. Song, X. Li, X. Wu, N. Brown, D. Maud, C. Naud, and W. A. de Heer, Phys. Status Solidi A **204**, 1746 (2007).
[24]M. Rubio-Roy, F. Zaman, Y. Hu, C. Berger, M. W. Moseley, J. D. Meindl, and W. A. de Heer, Appl. Phys. Lett. **96**, 082112 (2010).
[25]A. Reina, X. Jia, J. Ho, D. Nezich, H. Son, V. Bulovic, M. S. Dresselhaus, and J. Kong, Nano Lett. **9**, 30 (2009).
[26]Q. Yu, J. Lian, S. Siriponglert, H. Li, Y. P. Chen, and S.-S. Pei, Appl. Phys. Lett. **93**, 113103 (2008).
[27]K. S. Kim, Y. Zhao, H. Jang, S. Y. Lee, J. M. Kim, K. S. Kim, J.-H. Ahn, P. Kim, J.-Y. Choi, and B. H. Hong, Nature (London) **457**, 706 (2009).
[28]S. Stankovich, D. A. Dikin, G. H. B. Dommett, K. M. Kohlhaas, E. J. Zimney, E. A. Stach, R. D. Piner, S. T. Nguyen, and R. S. Ruoff, Nature (London) **442**, 282 (2006).
[29]S. Stankovich, D. A. Dikin, R. D. Piner, K. A. Kohlhaas, A. Kleinhammes, Y. Jia, Y. Wu, S. T. Nguyen, and R. S. Ruoff, Carbon **45**, 1558 (2007).
[30]R. F. Parvizi, D. Teweldebrhan, S. Ghosh, I. Calizo, A. A. Balandin, H. Zhu, and R. Abbaschian, Micro & Nano Letters, IET **3**, 29 (2008).
[31]L. Jiao, B. Fan, X. Xian, Z. Wu, J. Zhang, and Z. Liu, J. Am. Chem. Soc. **130**, 12612 (2008).
[32]A. C. Ferrari, J. C. Meyer, V. Scardaci, C. Casiraghi, M. Lazzeri, F. Mauri, S. Piscanec, D. Jiang, K. S. Novoselov, S. Roth, and A. K. Geim, Phys. Rev. Lett. **97**, 187401 (2006).
[33]A. Gupta, G. Chen, P. Joshi, S. Tadigadapa, and P. C. Eklund, Nano Letters **6**, 2667 (2006).
[34]I. Calizo, F. Miao, W. Bao, C. N. Lau, and A. A. Balandin, Appl. Phys. Lett. **91**, 071913 (2007).
[35]I. Calizo, A. A. Balandin, W. Bao, F. Miao, and C. N. Lau, Nano Lett. **7**, 2645 (2007).
[36]M. A. Pimenta, G. Dresselhaus, M. S. Dresselhaus, L. G. Cançado, A. Jorio, and R. Saito, Phys. Chem. Chem. Phys. **9**, 1276 (2007).
[37]I. Calizo, I. Bejenari, M. Rahman, G. Liu, and A. A. Balandin, J. Appl. Phys. **106**, 043509 (2009).
[38]I. Calizo, W. Bao, F. Miao, C. N. Lau, and A. A. Balandin, Appl. Phys. Lett. **91**, 201904 (2007).
[39]Y. Y. Wang, Z. H. Ni, T. Yu, Z. X. Shen, H. M. Wang, Y. H. Wu, W. Chen, and A. T. Shen Wee, J. Phys. Chem. C **112**, 10637 (2008).
[40]R. Abbaschian, L. Abbaschian, and R. E. Reed-Hill, *Physical Metallurgy Principles*, 4th ed. (Cengage Learning, Stamford, CT, 2009).
[41]E. Spiecker, A. K. Schmid, A. M. Minor, U. Dahmen, S. Hollensteiner, and W. Jäger, Phys. Rev. Lett. **96**, 086401 (2006).
[42]T. G. Kollie, Phys. Rev. B **16**, 4872 (1977).
[43]N. Mounet and N. Marzari, Phys. Rev. B **71**, 205214 (2005).
[44]W. Bao, F. Miao, Z. Chen, H. Zhang, W. Jang, C. Dames, and C. N. Lau, Nat. Nanotechnol. **4**, 562 (2009).
[45]H. O. Pierson, *Handbook of Carbon, Graphite, Diamond and Fullerenes: Properties, Processing, and Applications* (Noyes, Park Ridge, NJ).
[46]M. W. Barsoum, A. Murugaiah, S. R. Kalidindi, T. Zhen, and Y. Gogotsi, Carbon **42**, 1435 (2004).
[47]P. Thrower, in *Chemistry and Physics of Carbon*, edited by P. Walker (Marcel Dekker, New York).
[48]D. Graf, F. Molitor, K. Ensslin, C. Stampfer, A. Jungen, C. Hierold, and L. Wirtz, Nano Lett. **7**, 238 (2007).
[49]F. P. Incropera and D. P. DeWitt, *Introduction to Heat Transfer*, 4th ed. (Wiley, New York, 2002).
[50]P. Subramanian and D. Laughlin, *Phase diagrams of binary copper alloys*, Monograph Series on Alloy Phase Diagrams (ASM International, Materials Park, OH, 1994), Vol. 10, p. 109.
[51]M. Singleton and P. Nash, J. Phase Equilib. **10**, 121 (1989).
[52]J. M. Blakely, Crit. Rev. Solid State Mater. Sci. **7**, 333 (1978).
[53]M. Eizenberg and J. M. Blakely, J. Chem. Phys. **71**, 3467 (1979).
[54]M. Eizenberg and J. M. Blakely, Surf. Sci. **82**, 228 (1979).
[55]L. C. Isett and J. M. Blakely, Surf. Sci. **47**, 645 (1975).
[56]L. C. Isett and J. M. Blakely, J. Vac. Sci. Technol. **12**, 237 (1975).
[57]J. C. Shelton, H. R. Patil, and J. M. Blakely, Surf. Sci. **43**, 493 (1974).
[58]L. C. Isett and J. M. Blakely, Surf. Sci. **58**, 397 (1976).
[59]For a review see A. A. Balandin, IEEE Spectrum 29 (Oct. 2009).